Study of Protein Facilitated Water and Nutrient Transport in Plant Phloem

Tsun-kay Jackie Sze
School of Mechanical and Materials Engineering,
Washington State University,
Pullman, WA 99164

Prashanta Dutta[1]
School of Mechanical and Materials Engineering,
Washington State University,
Pullman, WA 99164
e-mail: dutta@mail.wsu.edu

Jin Liu
School of Mechanical and Materials Engineering,
Washington State University,
Pullman, WA 99164

Biological systems use transporter proteins to create concentration gradients for a variety of purposes. In plant, sucrose transporter proteins play a vital role in driving fluid flow through the phloem by generating chemical potential. In this study, we investigate these nanoscale phenomena of protein directed active transport in a microscale biological system. We presented a mathematical model for protein facilitated sucrose loading considering six different states of the sucrose transporter protein. In addition, we developed a quasi-one dimensional transport model to study protein facilitated pumping mechanisms in plant phloem. Here we specifically study the influence of transporter protein reaction rates, apoplast proton concentration, membrane electrical potential, and cell membrane hydraulic permeability on flow through the phloem. This study reveals that increasing companion cell side deprotonation rate significantly enhances the sieve tube sugar concentrations, which results in much higher water transport. Lower apoplast p*H increases the transport rate, but the flow control is less noticeable for a* p*H less than 5. A more negative membrane electrical potential difference will significantly accelerate the transporter proteins' ability to pump water and nutrients. Higher companion cell and sieve element membrane hydraulic permeability also promotes flows through the phloem; however, the flow difference is less noticeable at higher permeabilities when near typical plant cell membrane ranges.* [DOI: 10.1115/1.4026519]

Keywords: proton sucrose transporter proteins, sugar transport, quasi-one dimensional model, numerical model

1 Introduction

Plants transport nutrients and water through networks of cells called the xylem and phloem. Sugars and ions are transported from sources such as leaves to sinks (e.g., fruits, flowers, and roots) through the phloem. In order to transport nutrients, certain plants use active loading which is facilitated by sugar transporter proteins. The active loading of sugars into the sieve tube results in higher sugar concentration inside the sieve tube. The high solute concentration results in high osmotic pressure at the source, while unloading of solutes will lead to low osmotic pressure at sinks [1]. This induced pressure gradient will then drive fluid flow through the sieve tube from sources to sinks without requiring an external pump. The protein facilitated active loading of sugars enables plants to maintain steady sugar transport rates with low leaf sugar concentration, which allow for faster plant growth and less feedback inhibition of photosynthesis [2].

In addition to understanding transport of water and nutrients in plants, knowledge of protein actuated transport mechanisms can help in developing biomimetic engineering device. For instance, transporter proteins can potentially be used in many engineering systems due to their capability to generate solute concentration gradients while being on the nanoscale. Sundaresan and Leo used ATPase for power generation, where ATP is used to generate an ionic gradient across an artificial membrane which is then converted into electrical energy [3]. They used sucrose transporter protein to drive an actuator [4], which is proposed as a novel method to develop deformable smart materials. Compared to biomimetic engineering devices, which are still in development, plants are highly effective at using these nanoscale transporter proteins in microscale systems such as in the phloem.

Plant phloem is a complex system consisting of sieve elements, companion cells (CCs), phloem fibers, and phloem parenchyma. Different approaches have been used to model the transport of nutrients through the phloem. Most models consider sugar addition as functions that are dependent on sugar concentration [1,5]; however, these arbitrary functions are not able to describe the actual mechanism. Active loading was studied using Michaelis–Menten kinetics based on sucrose transporter measurements [6], but this model did not consider the effect from solute concentrations inside of the phloem.

In this work, we presented a comprehensive mathematical model to estimate the sucrose transport from the low concentration apoplast to the cytoplasm of companion cells and eventually to the sieve tube to understand the role and mechanism of these nanoscale transporter proteins. We modeled active loading through a six-state sucrose transporter protein and studied the nanoenvironment around the transporter protein. We investigated the dynamics of transporter proteins by modeling the plant phloem. To study the effects of transporter proteins in system level behavior, we presented quasi-1D governing equations by applying mass and momentum conservation principles in the phloem. The influences of the sucrose transporter deprotonation rate, apoplast *p*H, membrane electrical potential difference, and phloem cell membrane hydraulic permeability on flow through the phloem are then investigated using the proposed model.

2 Model Problem

To simulate the dynamics of transporter proteins in a biological system, we modeled the plant phloem as a single sieve tube including the sieve elements and neighboring companion cells for sugar transport from source to sink. We considered three zones representing different segments of the plant as shown in Fig. 1(*a*). In the loading zone (leafs), sugars are added by active loading

[1]Corresponding author.

Manuscript received January 8, 2014; final manuscript received January 15, 2014; published online February 19, 2014. Assoc. Editor: Sushanta K Mitra.

Copyright © 2013 by ASME

Downloaded From: http://nanoengineeringmedical.asmedigitalcollection.asme.org/ on 04/22/2014 Terms of Use: http://asme.org/terms

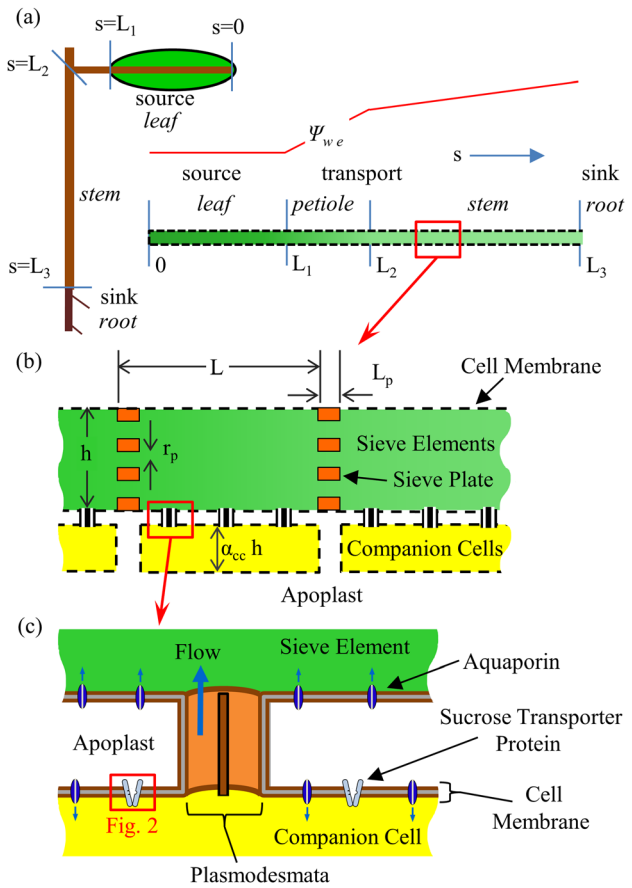

Fig. 1 (*a*) Transport of sugar and water through the four regions of sieve tube: a source region represented as leaf, transport region through the petiole, transport region through the stem, and unloading region in the root. (*b*) The sieve tube consists of sieve elements with sieve plates separating individual elements. We consider each sieve element with a length *L* and height *h*. Sieve plates have a thickness L_p and a sieve plate pore radius r_p. Water flows through the membrane from the surrounding apoplast (blank space) into the sieve element and neighboring companion cell. (*c*) Companion cells are considered as interconnected with neighboring sieve elements by plasmodesmata approximated as annular pores. The companion cell and sieve element cell are separated from the apoplast by the cell membrane, which contains aquaporins. It is assumed that the sugar transporter proteins are only present at the membrane of companion cell. The sucrose transporter protein and its different states are further illustrated in Fig. 2.

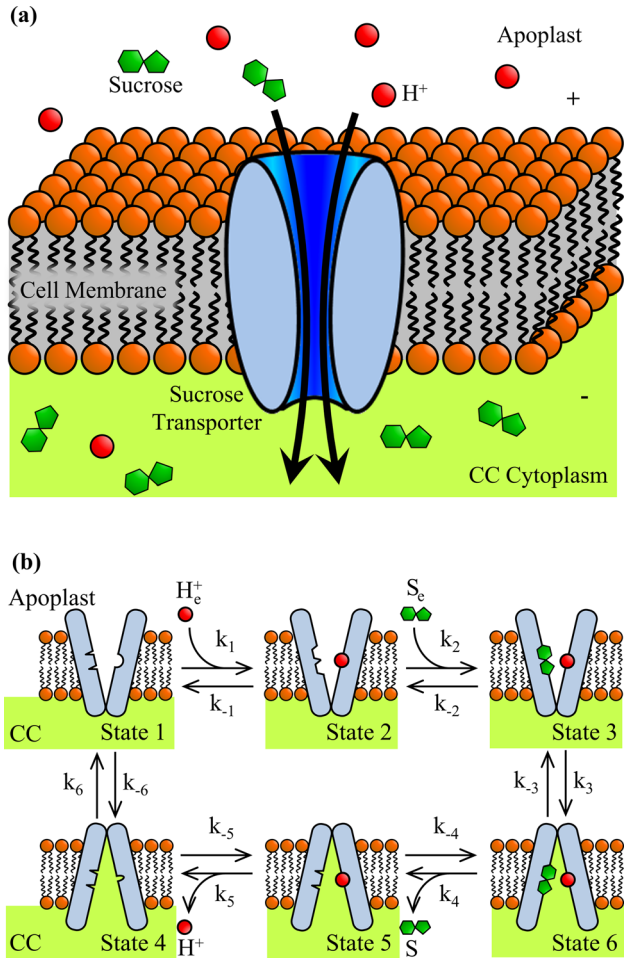

Fig. 2 (*a*) Proton sucrose transporter protein, where sucrose molecules are moved from the apoplast into the cytoplasm of the companion cell (CC). (*b*) Individual protein states during active loading of sucrose from the apoplast to the CC. There are a total of six states with 12 rate constants composed of forward k_n and reverse k_{-n} reactions. Reactant concentrations on both sides of the membrane are included, where the apoplast side sucrose concentration is S_e and the companion cell side sucrose concentration is *S*. Since the companion cell is connected to the sieve element (Fig. 1(*c*)), it is assumed that both companion cell and sieve element have the same reactant concentrations.

with the aid of a proton sucrose symporter. The second and third segments make up the transport zone represented as the petiole and stem, respectively. At the end of the modeled sieve channel we assumed that all sugars are unloaded, hence modeling of the unloading zone is not needed. Figure 1(*b*) shows sieve elements, which are connected with porous plates called sieve plates. Sieve elements are connected to neighboring companion cells by plasmodesmata, nanoscale pores, shown in Fig. 1(*c*). Thus, it was assumed that at any location the solute concentration and electric potential are the same for neighboring sieve elements and companion cells. The cytoplasms of the companion cells and sieve elements are separated from the apoplast by a cell membrane. The apoplast incorporates space outside of the plasma membrane, where for most parts solutes and water can diffuse through freely.

Plant cell membranes contain nanoscale water channels called aquaporins. Aquaporins have angstrom size pores [7] that allow water molecules to pass through, but restrict charged and larger molecules. As a result, water can be transferred between the apoplast and the companion cell or sieve element depending on pressure differences. Certain plants use active loading through sugar transporter proteins in their cell membrane to generate osmotic pressure. For instance, Solanaceae plants (including potato, tomato, and tobacco) have sugar transporter proteins located at the membrane separating the apoplast and the companion cells (Fig. 1(*c*)). The combined osmotic and thermodynamic pressures will determine the water potential Ψ_w which is the main driving force in plant transport.

3 Mathematical Model

3.1 Protein Activated Sugar Transport. In the case of plant phloem, sugars such as sucrose are driven from low concentration to high concentration through use of an electrochemical gradient facilitated by nanoscale transporter proteins. Most identified sucrose transporters to date are proton sucrose symporters [8]. Figure 2(*a*) shows a proton sucrose symporter, where both the proton and sucrose molecule move in the same direction. The proton gradient across the cell membrane is actively maintained by proton pumps moving protons from the cytoplasm to the apoplast. Due to the more negative electrical potential in the companion

Downloaded From: http://nanoengineeringmedical.asmedigitalcollection.asme.org/ on 04/22/2014 Terms of Use: http://asme.org/terms

cell cytoplasm compared to the surrounding apoplast, the positively charged protons will experience a force towards companion cell cytoplasm. This electrochemical potential is used to move the proton along with a sucrose molecule into the companion cell cytoplasm.

In this study, we modeled the active loading of sugar using six states as illustrated in Fig. 2(*b*). There are 12 rate constants to account for the forward and backward reactions. For the forward reaction starting at protein state 1, where the transporter protein is open to the apoplast, a proton from the apoplast first binds to the transporter protein. The protonation of the transporter protein will cause structural changes, which opens the binding site for sucrose molecules as shown in state 2. Sucrose molecules in the apoplast will then be attracted to the binding site and bind to the transporter protein (state 3). This leads to structural changes and opens the transporter protein towards the companion cell cytoplasm (state 4). The sucrose molecule then detaches from the transporter protein and enters the cytoplasm, which results in state 5. Once the sucrose molecule has left, the proton enters the cytoplasm and results in state 6. Finally, the cycle is completed by the transporter protein opening to the apoplast and exposing proton binding site (state 1).

Using the law of mass action, the accumulation rates of protein at different states can be expressed as

$$\begin{aligned}
\frac{dC_1}{dt} &= k_6C_6 - k_{-6}C_1 + k_{-1}C_2 - k_1C_1H_e^+ \\
\frac{dC_2}{dt} &= k_1C_1H_e^+ - k_{-1}C_2 + k_{-2}C_3 - k_2C_2S_e \\
\frac{dC_3}{dt} &= k_2C_2S_e - k_{-2}C_3 + k_{-3}C_4 - k_3C_3 \\
\frac{dC_4}{dt} &= k_3C_3 - k_{-3}C_4 + k_{-4}C_5S - k_4C_4 \\
\frac{dC_5}{dt} &= k_4C_4 - k_{-4}C_5S + k_{-5}C_6H^+ - k_5C_5 \\
\frac{dC_6}{dt} &= k_5C_5 - k_{-5}C_6H^+ + k_{-6}C_1 - k_6C_6
\end{aligned} \tag{1}$$

where k's are rate constants, C_m is the surface density of sucrose transporter proteins on the cell membrane at the mth state, S_e is the sucrose concentration on the apoplast side, S is the sucrose concentration on the companion cell side, and H^+ is the proton concentration on the companion cell side. We consider the reaction is at steady state and the total surface density of sucrose transporters C_o as constant. Hence, the density of proteins at each state can be solved in terms of rate constants and reactant (proton and sucrose) concentrations. The rate of sugar molecules moved into the sieve by the sucrose transporter can be expressed as

$$J_{\text{suc}} = k_4C_4 - k_{-4}C_5S \tag{2}$$

By solving Eq. (1) for protein densities and substituting the solution into Eq. (2), we get

$$J_{\text{suc}} = C_o\frac{H_e^+S_ek_1k_2k_3k_4k_5k_6 - H^+Sk_{-1}k_{-2}k_{-3}k_{-4}k_{-5}k_{-6}}{\Phi(k_m, k_{-m}, H_e^+, H^+, S_e, S)} \tag{3}$$

where Φ is a function of rate constants and reactant concentrations [11]. In this model, active loading is assumed to occur only on companion cells. Hence, the sucrose flux is calculated for companion cells and then converted for sieve wall as

$$J_{SwL} = J_{\text{suc}}\alpha_{mv}2\left(L - L_p + h\alpha_{\text{cc}L}\right)/L \tag{4}$$

where J_{SwL} is the sieve wall sucrose flux, $\alpha_{\text{cc }L}$ is the companion cell to sieve element height ratio in the loading zone, and α_{mv} is a factor accounting for wall ingrowths which increase cell surface area.

3.2 Quasi One-Dimensional Equations for Plant Phloem. The characteristic dimension of a sieve element ranges from nm (sieve pore radius, 100–1000 nm) to mm (sieve element, 100–1000 μm). Thus it is not possible to resolve all scales in a reasonable computation time. To investigate the effect of important parameters such as sucrose concentration, proton concentration, and electrical potential in the transporter protein nanoenvironment, we developed a quasi-one dimensional model considering each sieve element as one control volume. To derive our phloem transport model, we made the following assumptions:

(1) The fluid flow takes place in the sieve elements, and the sieve channel height (h) is constant.
(2) Flow is laminar; thus, fluid flow will quickly approach parabolic and can be approximated as a parabolic profile for regions apart from the sieve plate.
(3) Sieve plate pores are considered as cylindrical pores with equal size.
(4) Sucrose is the primary solute in the phloem sap, and the fluid properties only depend on sucrose concentration.
(5) The cross-stream pressure and sucrose concentration variations are sufficiently small such that streamwise (s) differences dominate.
(6) The sieve element and companion cells have the same solute concentration and electric potential since they are thoroughly connected by plasmodesmata.

3.2.1 Quasi One-Dimensional Continuity Equation. The conservation of mass (continuity) for a control volume is given as

$$\frac{\partial(m)_{\text{cv}}}{\partial t} = \sum_{\text{in}}\dot{m} - \sum_{\text{out}}\dot{m} \tag{5}$$

where $(m)_{\text{cv}}$ is the mass within the control volume and $\dot{m}$ is the mass flow rate. As shown in Fig. 3(*a*), we consider a two-dimensional control volume with a differential length Δs. By using integral form in the channel height direction (y), the continuity equation can be expressed as

$$\frac{\partial}{\partial t}\int_h \rho dy\Delta s = \int_h \rho u dy + \Delta\dot{m}_{\text{wall}} - \int_h\left[\rho u + \frac{\partial}{\partial s}(\rho u)\Delta s\right]dy \tag{6}$$

where h is the sieve element channel height.

The left hand side term of Eq. (6) represents the mass accumulation rate in the control volume. While the first, second, and third term of the right hand side represent mass influx through left boundary, mass flux through the wall ($\Delta\dot{m}_{\text{wall}}$), and the mass outflux through right boundary, respectively. Mass flux across the wall can be divided into two terms: mass added due to sugar influx ($\varpi J_{Sw}\Delta s$) and due to cell membrane water flow ($\rho_{\text{w}}v_{\text{w}}f\Delta s$), where v_{w} is the wall flow velocity, J_{Sw} is the sucrose influx, f is a geometrical factor accounting for the sieve plate, and ϖ is the molecular mass of sucrose. Assuming constant sap (fluid) properties across the channel, the continuity equation becomes

$$\frac{\partial}{\partial t}\rho h + \frac{\partial}{\partial s}(\rho\bar{u})h - \rho_{\text{w}}v_{\text{w}}f - \varpi J_{Sw} = 0 \tag{7}$$

where $\bar{u}(s)$ is the average velocity at a location s. If we assume a parabolic velocity profile in the sieve element, the relationship between average velocity and 2D flow velocity becomes

$$u(s,y) = \bar{u}(s)\frac{6}{h}\left(y - \frac{y^2}{h}\right) \tag{8}$$

Downloaded From: http://nanoengineeringmedical.asmedigitalcollection.asme.org/ on 04/22/2014 Terms of Use: http://asme.org/terms

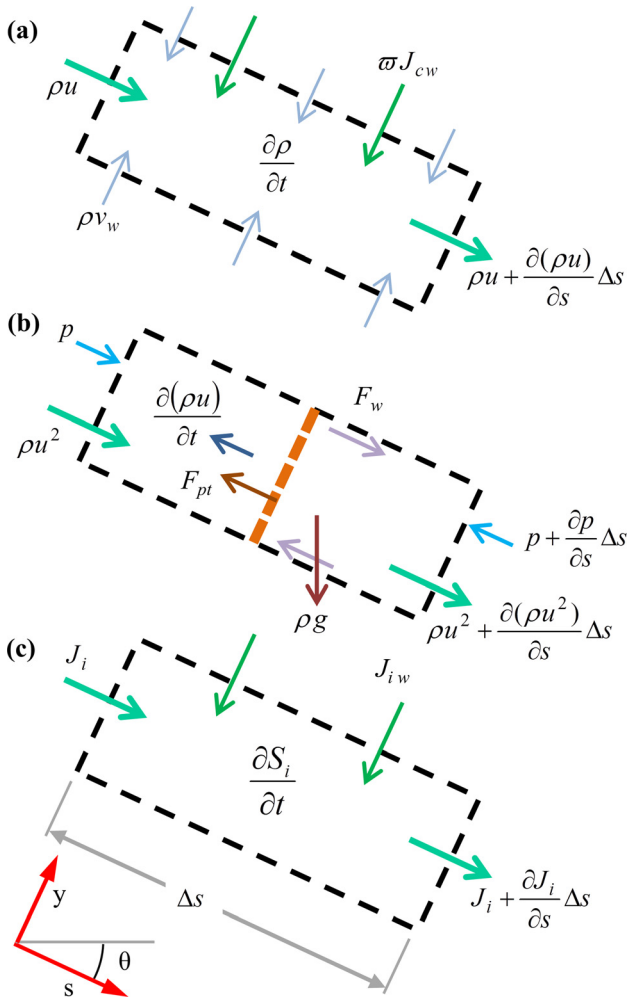

Fig. 3 Schematic of control volumes used in this model for (*a*) continuity, (*b*) momentum, and (*c*) chemical species mass conservation equations. For continuity we consider mass added due to streamwise flow, sugar loaded, and water loaded by osmotic pressures. The momentum equation includes forces due to thermodynamic pressure, wall shear stress, sieve plate drag, and additional body forces. In the case of the mass conservation equation for chemical species, we consider streamwise species flux and flux due to species loading.

3.2.2 Quasi One-Dimensional Momentum Equation. Starting from the Newton's second law, the momentum equation for a control volume in the s direction is given as

$$\sum F = \frac{\partial}{\partial t}(mu)_{\mathrm{cv}} - \sum_{\mathrm{in}} \dot{m}u + \sum_{\mathrm{out}} \dot{m}u \tag{9}$$

For the momentum equation, we consider again a control volume of size Δs and integral form in the y direction as shown in Fig. 3(*b*). Since the channel height is constant, the momentum flux from the wall mass flux will not contribute. Thus, the rate in change of momentum within the control volume will be

$$\frac{\partial}{\partial t}\int_h \rho u \mathrm{d}y \Delta s - \int_h \rho u^2 \mathrm{d}y + \int_h \left[\rho u^2 + \frac{\partial}{\partial s}(\rho u^2)\Delta s\right]\mathrm{d}y \tag{10}$$

The various forces involved in the transport of sap includes the force from the thermodynamic pressure, cell wall shear stress, body force (such as gravity but can be expanded for other terms), and drag force from the sieve plate. The resultant forces can be expressed as

$$-\frac{\partial}{\partial s}\int_h p \mathrm{d}y \Delta s + F_{\mathrm{w}} + \int_h \rho g \mathrm{d}y \Delta s \sin\theta + F_{\mathrm{pt}} \tag{11}$$

By inserting Eqs. (10) and (11) into Eq. (9) the momentum equation becomes

$$\begin{aligned} &-\frac{\partial}{\partial s}\int_h p \mathrm{d}y \Delta s + F_{\mathrm{w}} + \int_h \rho g \mathrm{d}y \Delta s \sin\theta + F_{\mathrm{pt}} \\ &= \frac{\partial}{\partial t}\int_h \rho u \mathrm{d}y \Delta s + \int_h \frac{\partial}{\partial s}(\rho u^2)\mathrm{d}y \Delta s \end{aligned} \tag{12}$$

Next we determine the drag forces from wall shear stress and sieve plates. The force from wall shear stress can be found as

$$F_{\mathrm{w}} = \mu \frac{\partial u}{\partial y}\bigg]_{y=h} \Delta s - \mu \frac{\partial u}{\partial y}\bigg]_{y=0} \Delta s \tag{13}$$

Using Darcy's Law, the drag force from the sieve plate resisting fluid flow is

$$F_{\mathrm{pt}} = -\int_h \frac{\mu u}{K}\mathrm{d}y \Delta s \tag{14}$$

where K is a permeability factor. Wang provided a solution for stokes flow through a porous plate [9]

$$K = \frac{L r_{\mathrm{p}} \beta}{\xi_1(\beta, L_{\mathrm{p}}, r_{\mathrm{p}})\pi} \tag{15}$$

$$\xi_1(\beta, L_{\mathrm{p}}, r_{\mathrm{p}}) = 3 + \frac{16}{\pi}\left(\frac{L_{\mathrm{p}}}{2r_{\mathrm{p}}}\right) - \xi_2(\beta) \tag{16}$$

where L is the length of the sieve element, L_{p} is the sieve plate thickness, r_{p} is the sieve plate pore radius, and β is the sieve plate porosity. The first term in the right hand side of Eq. (16) accounts for resistance relating to a pore in a thin plate, the second term accounts for the effect of pore thickness, and the third term ξ_2 is accounting for the effect of neighboring pores. At a porosity of 0, the sieve plate will be completely blocked. By fitting a fourth order polynomial, the ξ_2 term from Ref. [9] can be approximated as

$$\xi_2(\beta) = 2.6924\beta^4 - 4.3341\beta^3 + 3.6075\beta^2 - 0.26702\beta + 0.070413 \tag{17}$$

The force terms in Eqs. (13) and (14) are substituted into Eq. (12) to obtain a quasi-1D momentum equation, given as

$$\frac{\partial}{\partial t}(\rho \bar{u}) = -\frac{\partial p}{\partial s} - 12\frac{\mu \bar{u}}{h^2} + \rho g \sin\theta - \frac{\mu \bar{u}}{K} - 1.2\frac{\partial}{\partial s}(\rho \bar{u}^2) \tag{18}$$

3.2.3 Quasi One-Dimensional Mass Conservation Equation for Chemical Species. The mass balance for a chemical species i is given as

$$\frac{\partial (m_i)_{\mathrm{cv}}}{\partial t} = \sum_{\mathrm{in}} \dot{m}_i - \sum_{\mathrm{out}} \dot{m}_i \tag{19}$$

where $(m_i)_{\mathrm{cv}}$ is the mass of the ith species within the volume and $\dot{m}_i$ is the mass flow rate. For the control volume shown in Fig. 3(*c*), the mass conservation of chemical species can be written as

$$\frac{\partial}{\partial t}\int_h S_i \mathrm{d}y \Delta s = \int_h J_i \mathrm{d}y + J_{iw}\Delta s - \int_h \left[J_i + \frac{\partial J_i}{\partial s}\Delta s\right]\mathrm{d}y \tag{20}$$

Downloaded From: http://nanoengineeringmedical.asmedigitalcollection.asme.org/ on 04/22/2014 Terms of Use: http://asme.org/terms

Table 1 Boundary conditions for full sieve tube simulation

Boundary condition	Governing equation
$D\partial S/\partial s - \bar{u}S = 0 \quad \text{for} \quad s = 0$	Equation (22)
$\partial S/\partial s = 0 \quad \text{for} \quad s = L_3$	Equation (22)
$\bar{u} = 0 \quad \text{for} \quad s = 0$	Equations (7) and (18)
$P = P_{\text{out}} \quad \text{for} \quad s = L_3$	Equations (7) and (18)
$\partial \bar{u}/\partial s = 0 \quad \text{for} \quad s = L_3$	Equations (7) and (18)

where S_i is the concentration of species i, J_i is the flux of species in the s direction, and $J_{i\ w}$ is the flux of species through the top wall. Species flux is composed of three terms including advection, diffusion, and electromigration

$$J_i = uS_i - D\left(\frac{\partial S_i}{\partial s} - \frac{z\Gamma}{RT}S_i\frac{\partial \phi}{\partial s}\right) \tag{21}$$

By substituting Eq. (21) into Eq. (20) for species flux along the tube and then integrating in y direction, the quasi-1D mass conservation equation for chemical species becomes

$$\frac{\partial}{\partial t}S_i h + \frac{\partial}{\partial s}\left[\bar{u}S_i - D\left(\frac{\partial S_i}{\partial s} - \frac{z\Gamma}{RT}S_i\frac{\partial \phi}{\partial s}\right)\right]h - J_{iw} = 0 \tag{22}$$

In this paper sucrose is assumed as the primary solute; hence, we only solve for sucrose concentration (S) in the channel. Although sucrose molecules are electroneutral, we keep our governing equation general to allow for future analysis into transport of charged ions (such as potassium).

3.2.4 Auxiliary Conditions. The boundary conditions are summarized in Table 1. For the sucrose mass conservation equation, there will be no sucrose flux at the starting end and no sugar gradient at the sink end. For continuity and momentum equations, at the starting end we consider no fluid flow; at the sink end, we fixed thermodynamic pressure with fully developed flow.

Wall flow through the cell membrane into the sieve and companion cells is driven by pressure gradients and is governed by the Kedem and Katchalsky equation [10]

$$v_m = M_{\text{p}}[p_e - p - \sigma(\Pi(S_e) - \Pi(S))] \tag{23}$$

where M_{p} is the membrane hydraulic permeability accounting for all membrane properties, σ is the membrane reflection coefficient which is assumed as 1 in our simulations, v_m is the flow through the membrane towards the internal side, $\Pi(S)$ is the internal side osmotic pressure, and $\Pi(S_e)$ is the apoplast side osmotic pressure. Sieve wall flow velocity is calculated from two terms: direct flow ($v_{\text{ext}\to\text{sieve}}$) from the apoplast into the sieve element and indirect flow ($v_{\text{ext}\to\text{CC}\to\text{sieve}}$) from the apoplast into the companion cell then into the sieve element

$$v_{\text{w}} = 2v_{\text{ext}\to\text{sieve}} + v_{\text{ext}\to\text{CC}\to\text{sieve}} \tag{24}$$

Direct inflow is calculated from Eq. (23) using the sieve pressures as the internal side. Indirect flow can be calculated from Eq. (23) using companion cell pressures as inside and then converting to sieve wall flow. Companion cell pressures are estimated by approximating connecting plasmodesmata as annular pores described in the 2D model [11].

3.3 Fluid Properties. We treat the fluid (sap) as a sucrose water solution. All fluid properties are calculated based on sucrose concentration (S) in units of molal. Fluid density and viscosity are calculated from Ref. [12]

$$\rho = \rho_{\text{water}}(1 + 0.867S)^{0.164} \tag{25}$$

Table 2 Rate constants based on Ref. [18] with modifications to include companion cell side reactant concentrations. Rates for k_n^* can be calculated from membrane electrical potential as described in Ref. [18]. Rate k_5 is varied in certain simulations.

Forward reaction	Units	Reverse reaction	Units
$k_1^* = 7.0 \times 10^7$	$\text{M}^{-1}\ \text{s}^{-1}$	$k_{-1}^* = 2.3 \times 10^2$	s^{-1}
$k_2 = 1.7 \times 10^3$	$\text{M}^{-1}\ \text{s}^{-1}$	$k_{-2} = 5.0$	s^{-1}
$k_3 = 50$	s^{-1}	$k_{-3} = 50$	s^{-1}
$k_4 = 1.0 \times 10^3$	s^{-1}	$k_{-4} = 3.79 \times 10^2$	$\text{M}^{-1}\ \text{s}^{-1}$
$k_5 = 4.3$	s^{-1}	$k_{-5} = 1.41 \times 10^9$	$\text{M}^{-1}\ \text{s}^{-1}$
$k_6^* = 6.0$	s^{-1}	$k_{-6}^* = 5.0$	s^{-1}

$$\mu = \mu_{\text{water}}(1 + 0.867S)^{.164} \times \left[1 + 0.73S\exp\left(\frac{S^{1.1}}{8.345T/273.1 - 7.042}\right)\right] \tag{26}$$

We assume the temperature as 25 °C, so $\rho_{\text{water}} = 997.2\ \text{kg m}^{-3}$ and $\mu_{\text{water}} = 8.905 \times 10^{-4}\ \text{Pa s}$. The diffusion coefficient of sucrose molecules in the sap is estimated as [13,14]

$$D = 5.23 \times 10^{-10}\exp(-0.7248S) \tag{27}$$

In addition, osmotic pressure can be estimated as [15]

$$\Pi = RT\rho_{\text{water}}(0.998S + 0.089S^2) \tag{28}$$

4 Results and Discussion

The operation of the sucrose transporter protein is dependent on the properties on both sides of the membrane. We base simulations on typical apoplast pH ranges, from 4.5 to 6.5. We used an apoplast sucrose concentration of 2.1 mM [16] and a companion cell cytoplasm side pH of 7.5 [17]. The sucrose transporter is also influenced by the membrane electrical potential difference, and typical values for these potential differences range from −50 to −170 mV. Rate constants used in this model are listed in Table 2 with membrane electrical potential dependent steps following procedures from Ref. [18]. Sucrose transporter surface density is estimated as 0.12 proteins nm^{-2} based on companion cell sucrose flux ranges.

The simulation domain for our sieve tube includes the loading (with transporter proteins) and transport zones. The loading zone is modeled as active transport with sucrose transporter proteins and we assume no sugar influx in the transport zone

$$\begin{aligned} J_{Sw} &= J_{SwL} \quad s < L_1 \\ J_{Sw} &= 0 \quad\quad L_1 < s \end{aligned} \tag{29}$$

We also considered the orientation of different zones. The leaf and the petiole are assumed to be horizontal, while the stem is considered as vertical and the gravity will affect the flow through the stem. In addition, the companion cell sizes are different in the two zones. Companion cell sizes are based on measured ratios between sieve and companion cell height in different plant regions [19]. We considered the companion cell as 70% of the sieve height in the transport zone (α_{cc}) and 140% of the sieve height in the loading zone ($\alpha_{\text{cc}\ L}$). The sieve element is assumed to have same length as the companion cell. Companion cells in minor veins of certain active loaders have wall ingrowths that increase surface area [19]. These ingrowths increase surface area by 1.2 to 20 times. Hence, we increased source zone companion cell surface area α_{mv} by 4 times.

It has been observed that the flow velocities in the phloem of castor bean (*Ricinus communis*) *and* tobacco (*Nicotiana tabacum*) remain unchanged throughout the day [20]. Therefore we assume steady flow in our simulations, although our model can be easily

Downloaded From: http://nanoengineeringmedical.asmedigitalcollection.asme.org/ on 04/22/2014 Terms of Use: http://asme.org/terms

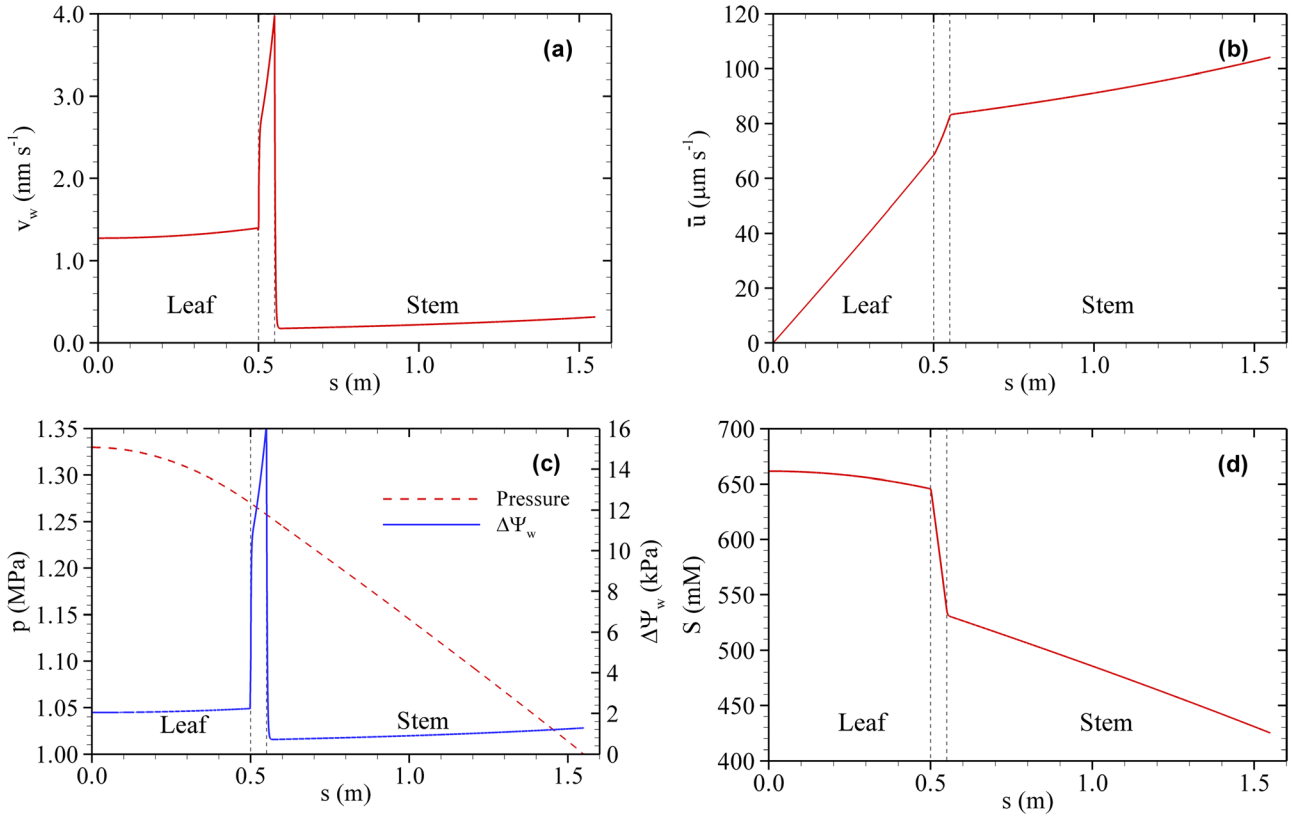

Fig. 4 Distribution along sieve tube for (*a*) wall flow velocity, (*b*) average velocity, (*c*) pressure and water potential difference, and (*d*) sucrose concentration. The modeled sieve tube is decomposed into three sections: leaf, petiole (between leaf and stem region), and stem. Simulation results are based on a k_5 of 4.3 s^{-1}, an apoplast *p*H of 6.1, a membrane electrical potential difference of −140 mV, and a cell membrane permeability of 6×10^{-14} m Pa^{-1} s^{-1}.

extended to study unsteady problems. Transport mechanics in the phloem is studied with an in-house numerical model solving for governing equations of the microscale system. Differential equations are solved with the semi-implicit method for pressure-linked equations using collocated storage [21–23]. For all simulations, the computational grids are set as 120 μm. In this section we investigate the influence of various parameters in transporter protein nanoenvironment on fluid transport through the phloem. The length of the loading zone (L_1) is set as 0.5 m based on sieve tube length used by other transport models [24]. The petiole is set as 5 cm long based on typical lengths [25]. In addition, the stem is set as 1 m tall based on tobacco plant heights [26].

Sieve element dimensions are based on tobacco with a length of 120 μm and height of 11 μm; the sieve plate is modeled with a thickness of 1.2 μm, a sieve plate pore radius of 0.35 μm and a sieve plate porosity (β) of 43.7% [27]. Plant cell membrane hydraulic permeability is based on typical plant cells which range from 1 to 400×10^{-14} m Pa^{-1} s^{-1}. Apoplast water potentials ($\Psi_{we} = p_e - \Pi(S_e)$) are set as −0.7 MPa for leaf, −0.3 MPa for the stem at L_2 (1 m above ground), and −0.2 MPa for the stem at L_3 (at soil surface) based on *N. tabacum* [26]. Apoplast water potential in the transport zone is varied as shown in Fig. 1(*a*). The thermodynamic pressure at the sink end of the sieve tube is set as 1 MPa based on typical sieve pressure ranges (of 0.8 to 1.4 MPa).

4.1 Distribution Through a Sieve Tube. The full sieve tube is simulated using boundary conditions described in Sec. 3.2.4 with the simulation domain shown in Fig. 1. Wall flow is shown in Fig. 4(*a*). In the loading zone (leaf), the direct addition of sugar due to active loading will result in a more negative water potential in the sieve element, which will cause wall flow from apoplast to sieve element. On the other hand, in the transport sections (petiole and stem), there is no sugar addition, and the water flow through wall membrane is due to changes in water potential difference between apoplast and sieve element. The wall flow increases sharply in the petiole section due to the sharp rise in apoplast water potential in that section (See Fig. 1(*a*)). In the stem region, wall flow occurs due to the gradual increase in apoplast water potential.

The average flow velocity in the sieve element will be the combination of wall flow and inflow, which is shown in Fig. 4(*b*). In the loading zone (leaf), the sugar influx and cell membrane water flow will increase mass transport through the sieve. This active transport of sugar molecules is the driving mechanism for flow through the phloem; as a result, flow velocity will increase the most in the loading zone. The high wall flow velocity in the petiole sieve will also lead to a noticeable increase in fluid flow. In the stem section, there will be a minor increase in velocity from the small amount of water flowing through the membrane into the sieve.

The thermodynamic pressure and water potential difference ($\Delta\Psi_w = \Delta\Psi_{w\,e} - \Delta\Psi_{w\,in}$) are shown in Fig. 4(*c*). Here the thermodynamic pressure is related to the flow velocity to conserve momentum in the sieve element. On the other hand, water potential difference is proportional to wall flow. There is a slight difference in proportion between wall flow and water potential in the loading zone. This difference is due to the companion cells having more surface area in the loading zone than the transport zone. Hence, a similar water potential difference will result in larger wall flow into the sieve for the loading zone when compared with the transport zone. Figure 4(*d*) shows the sucrose concentration distribution. In the loading zone, sugar is actively loaded which maintains a nearly constant sugar concentration. In the transport zone no sugars are loaded, hence wall flow will decrease sugar concentration. The higher wall flow in the petiole section will result in a

Downloaded From: http://nanoengineeringmedical.asmedigitalcollection.asme.org/ on 04/22/2014 Terms of Use: http://asme.org/terms

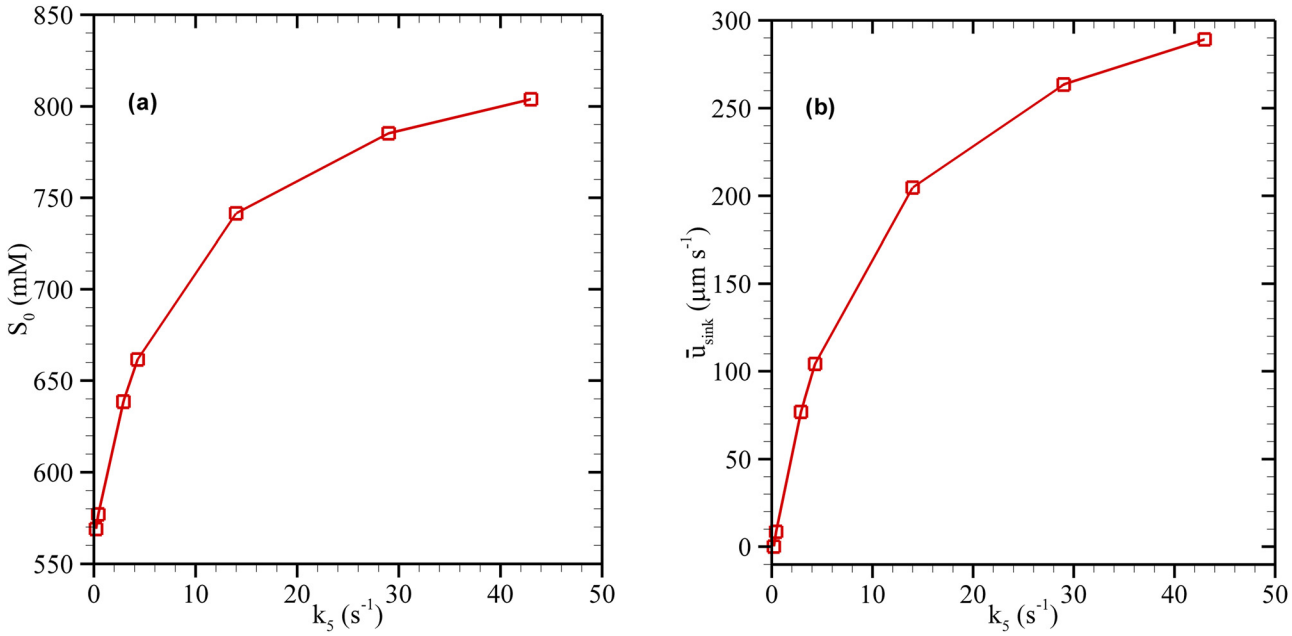

Fig. 5 Influence of companion cell side deprotonation rate constant k_5 on (*a*) sieve tube sugar concentration at starting end ($s = 0$) and (*b*) sieve tube average velocity at the sink end ($s = L_3$). All other conditions are the same as Fig. 4.

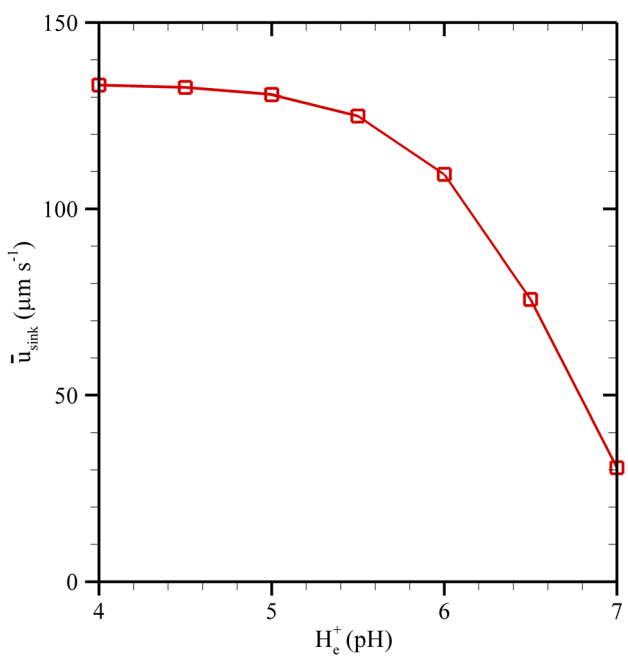

Fig. 6 The influence of apoplast proton concentration on fluid velocity at the sink end ($s = L_3$). All other conditions are the same as Fig. 4.

faster decrease in sieve sugar concentration, while the lower wall flow in the stem will result in a slower decrease in sugar concentration.

4.2 Companion Cell Side Deprotonation. We investigated the influence of sucrose transporter reaction steps on the efficacy of sucrose transporter proteins in pumping water and nutrient through the phloem. The rate limiting constant, in this case sucrose transporter deprotonation rate on the companion cell side (k_5), is varied. All other inputs are the same as the conditions used in Sec. 4.1. Figure 5(*a*) shows the loading zone sucrose concentration at different k_5. The sucrose transporter uses the proton gradient to move proton and sucrose molecules from low (apoplast) to high (companion cell) sugar concentration. At a higher value of k_5, the sucrose transporter protein will be capable of maintaining a larger sugar concentration gradient. This increase in osmotic pressure gradient across the membrane will drive larger flows. For this reason as k_5 increases, flow through the sieve tube will also increase as shown in Fig. 5(*b*). On the other hand, if the barrier to protons entering the cell is sufficiently large (low k_5) the sucrose concentration gradient will tend to drive protons and sucrose molecules in the reverse direction (from the cell to apoplast). Hence at a low k_5 the sucrose transporter will stop working, resulting in negligible flow. This study reveals that the water transport through the phloem can be regulated actively by modulating the deprotonation rate constants.

4.3 Apoplast *p*H. To illustrate the influence of reactant concentrations in pumping sugars from low concentration (apoplast) to high concentration (companion cell), we vary apoplast proton concentration from a *p*H of 4 to 7 with other inputs the same as Sec. 4.1. Figure 6 shows the relation between apoplast *p*H and flow velocity at the sink side of a sieve tube. As protons become readily available in the apoplast, the probability is higher for a proton to travel close enough with sufficient energy to attach to the binding site (Fig. 2(*b*), states 1 to 2). Hence protons will be able to pass to the companion cell side faster, which will help the transporter protein generate a larger sugar concentration gradient. As a result when there are more protons in the apoplast, the faster functioning of the sucrose transporter will increase fluid flow. Above a *p*H of 5, changes in apoplast *p*H result in noticeable differences in flow velocity. Plant apoplast *p*H can be actively changed depending on stimulus. It is possible that plants keep apoplast *p*H sufficiently high (above *p*H 5) to enable proton controlled sucrose fluxes. For engineering devices, the choice of *p*H range may be chosen depending on whether flow control is desired.

4.4 Membrane Electrical Potential Difference. Membrane electrical potential difference (ΔV_m) may also be a significant factor in the function of transporter proteins. We studied the influence of membrane electrical potential difference between the

Downloaded From: http://nanoengineeringmedical.asmedigitalcollection.asme.org/ on 04/22/2014 Terms of Use: http://asme.org/terms

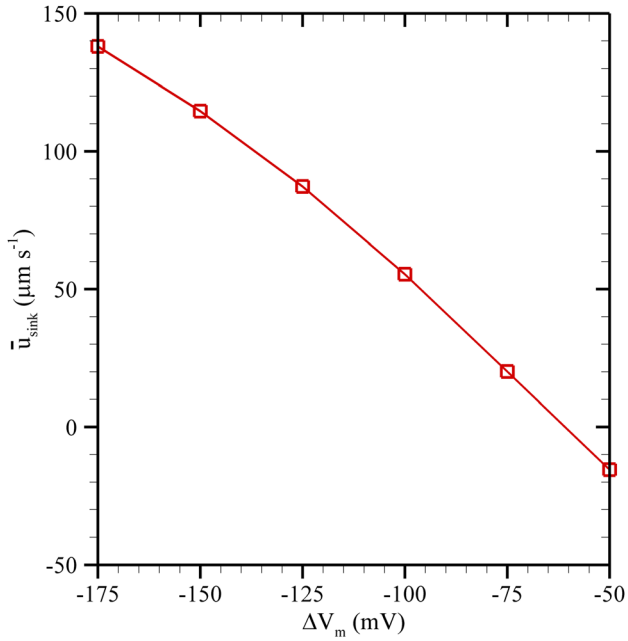

Fig. 7 The effect of membrane electrical potential difference on fluid velocity at the sink end ($s = L_3$). All other conditions are the same as Fig. 4. A more negative membrane electrical potential difference implies a more negative charge in the companion cell.

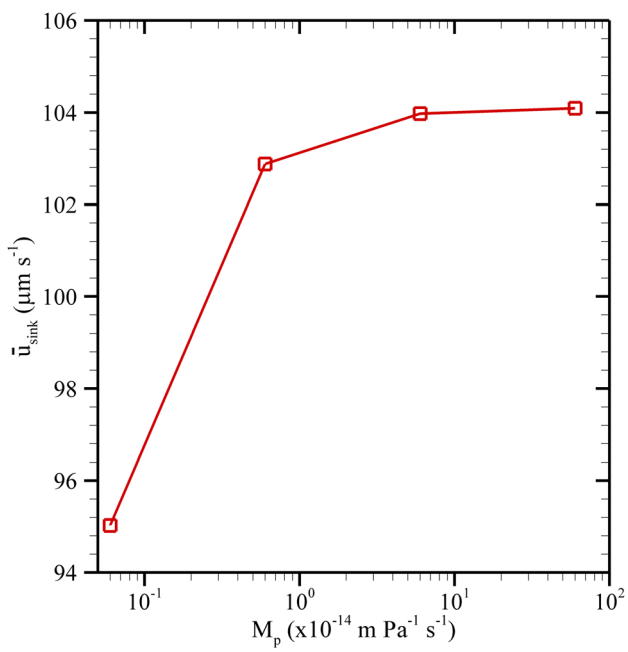

Fig. 8 Sieve tube average velocity at the sink end ($s = L_3$) for different cell membrane hydraulic permeabilities. All other conditions are the same as Fig. 4. Membrane hydraulic permeability is shown on a log scale.

apoplast and companion cell cytoplasm within plant ranges while keeping other parameters the same as Sec. 4.1. The effect of membrane electrical potential on the function of the proton sucrose transporter protein is shown in Fig. 7. The membrane electrical potential difference is the electrical potential inside the cell subtracted by the electrical potential outside the cell ($\Delta V_m = V_{in} - V_{out}$). Hence, a more negative electrical potential difference will drive positively charged protons inwards at a faster rate. With a larger proton flux, sugar influx will be faster which will lead to a higher sugar concentration gradient. Again, the higher sugar concentration gradient will result in faster transport through the sieve tube. Hence as membrane electrical potential becomes more negative fluid flow will increase. This study shows that within typical biological ranges (−50 to −170 mV), flow through the phloem is a strong function of electrical potential difference.

4.5 Cell Membrane Hydraulic Permeability (M_p). We also studied the effects of cell membrane hydraulic permeability. Companion cell and sieve element membrane hydraulic permeability are varied while keeping the other conditions same as Sec. 4.1. Figure 8 shows the influence of cell membrane hydraulic permeability on average velocity at the sink end. As the membrane becomes more permeable, a similar pressure force will result in larger wall flow. However, an increase in wall flow will reduce sieve side sucrose concentration and reduce driving osmotic pressures. In typical plant ranges, hydraulic permeability is sufficiently high and wall flow will be limited by pressure differences. It has been shown that under sufficiently watered conditions, water flow rates are similar between plants with and without reduced number of aquaporins [28]. As these nanoscale pores (aquaporins Fig. 1(*c*)) become more abundant, the hydraulic permeability will increase. Changes in hydraulic permeability will result in noticeable differences at lower permeabilities (when under 0.1×10^{-14} m Pa^{-1} s^{-1}). As a result, membrane hydraulic permeability may still be of interest for applications using artificially modified membranes.

5 Conclusions

In this paper we studied the effect of nanoscale sucrose transporter proteins and its nanoenvironment in a microscale system using a quasi-1D phloem model. We developed a mathematical model for protein facilitated active loading in sieve tube considering six different states of the transporter protein. We also developed a numerical model to simulate fluid flow through plant phloem based on quasi-1D governing equations. The numerical model is used to simulate the full sieve tube of a plant. Simulation results show that fluid flow increases most significantly at the location of active transport where sugar is added by sucrose transporter proteins. The influence of sucrose transporter reactions is studied by varying the rate limiting constant k_5. Our numerical model indicates that accelerating companion cell side deprotonation reaction rate will result in larger sucrose influx from apoplast to the companion cell and eventually to the sieve element. This increase in sucrose inside the sieve tube drives much larger water flows. We also studied the effect of apoplast proton concentration on the pumping ability of transporter proteins. At a higher apoplast proton concentration (lower apoplast *p*H), sucrose influx will also increase. Below a *p*H of 5, a change in apoplast *p*H will not modify the sucrose influx significantly. We also investigated the influence of membrane electrical potential on the transporter protein's ability to load sugar into the sieve tube. In typical plant ranges, varying membrane electrical potential difference will significantly alter the sugar transport rate. The impact of the cell membrane is also studied by changing companion cell and sieve element membrane hydraulic permeability. Although increasing membrane hydraulic permeability increases flow, the change is only noticeable at low hydraulic permeabilities. This study of the nanoscale transporter proteins and its nanoenvironment in a microscale biological system allows us to better understand the performance of these transporter proteins in engineering devices.

Acknowledgment

This work was supported in part by the National Science Foundation under Grant No. CBET 1250107.

Downloaded From: http://nanoengineeringmedical.asmedigitalcollection.asme.org/ on 04/22/2014 Terms of Use: http://asme.org/terms

References

[1] Lacointe, A., and Minchin, P. E. H., 2008, "Modelling Phloem and Xylem Transport Within a Complex Architecture," Funct. Plant Biol., **35**(10), pp. 772–780.

[2] Turgeon, R., 2010, "The Role of Phloem Loading Reconsidered," Plant Physiol., **152**(4), pp. 1817–1823.

[3] Sundaresan, V. B., and Leo, D. J., 2010, "Chemoelectrical Energy Conversion of Adenosine Triphosphate Using ATPases," J. Intell. Mater. Syst. Struct., **21**(2), pp. 201–212.

[4] Sundaresan, V. B., and Leo, D. J., 2008, "Modeling and Characterization of a Chemomechanical Actuator Using Protein Transporter," Sens. Actuators B, **131**(2), pp. 384–393.

[5] Jensen, K. H., Berg-Sørensen, K., Friis, S. M. M., and Bohr, T., 2012, "Analytic Solutions and Universal Properties of Sugar Loading Models in Münch Phloem Flow," J. Theor. Biol., **304**, pp. 286–296.

[6] De Schepper, V., and Steppe, K., 2010, "Development and Verification of a Water and Sugar Transport Model Using Measured Stem Diameter Variations," J. Exp. Bot., **61**(8), pp. 2083–2099.

[7] Kong, Y., and Ma, J., 2001, "Dynamic Mechanisms of the Membrane Water Channel Aquaporin-1 (AQP1)," Proc. Natl. Acad. Sci. U.S.A., **98**(25), pp. 14345–14349.

[8] Tang, C., Huang, D., Yang, J., Liu, S., Sakr, S., Li, H., Zhou, Y., and Qin, Y., 2010, "The Sucrose Transporter HbSUT3 Plays an Active Role in Sucrose Loading to Laticifer and Rubber Productivity in Exploited Trees of Hevea brasiliensis (para rubber tree)," Plant Cell Environ., **33**(10), pp. 1708–1720.

[9] Wang, C. Y., 2010, "Stokes Flow Through a Barrier With Distributed Pores," Chem. Eng. Commun., **197**(11), pp. 1428–1434.

[10] Kargol, M., and Kargol, A., 2003, "Mechanistic Equations for Membrane Substance Transport and their Identity With Kedem-Katchalsky Equations," Biophys. Chem., **103**(2), pp. 117–127.

[11] Sze, T.-k. J., Liu, J., and Dutta, P., 2013, "Numerical Modeling of Flow through Phloem Considering Active Loading," ASME J. Fluids Eng., **136**, p. 021206.

[12] Chenlo, F., Moreira, R., Pereira, G., and Ampudia, A., 2002, "Viscosities of Aqueous Solutions of Sucrose and Sodium Chloride of Interest in Osmotic Dehydration Processes," J. Food Eng., **54**(4), pp. 347–352.

[13] Ekdawi-Sever, N., de Pablo, J. J., Feick, E., and von Meerwall, E., 2003, "Diffusion of Sucrose and Alpha,Alpha-Trehalose in Aqueous Solutions," J. Phys. Chem. A, **107**, pp. 936–943.

[14] Chatterjee, A., 1964, "Measurement of the Diffusion Coefficients of Sucrose in Very Dilute Aqueous Solutions Using Jamin Interference Optics at 25 deg," J. Am. Chem. Soc., **86**(5), pp. 793–795.

[15] Michel, B. E., 1972, "Solute Potentials of Sucrose Solutions," Plant Physiol., **50**(1), pp. 196–198.

[16] Sweetlove, L. J., Kossmann, J., Riesmeier, J. W., Trethewey, R. N., and Hill, S. A., 1998, "The Control of Source to Sink Carbon Flux During Tuber Development in Potato," Plant J., **15**(5), pp. 697–706.

[17] Hafke, J. B., van Amerongen, J. K., Kelling, F., Furch, A. C., Gaupels, F., and Van Bel, A. J. E., 2005, "Thermodynamic Battle for Photosynthate Acquisition Between Sieve Tubes and Adjoining Parenchyma in Transport Phloem," Plant Physiol., **138**(3), pp. 1527–1537.

[18] Boorer, K. J., Loo, D. D., Frommer, W. B., and Wright, E. M., 1996, "Transport Mechanism of the Cloned Potato H+/Sucrose Cotransporter StSUT1," J. Biol. Chem., **271**(41), pp. 25139–25144.

[19] Kempers, R., Ammerlaan, A., and Van Bel, A. J. E., 1998, "Symplasmic Constriction and Ultrastructural Features of the Sieve Element/Companion Cell Complex in the Transport Phloem of Apoplasmically and Symplasmically Phloem-Loading Species," Plant Physiol., **116**(1), pp. 271–278.

[20] Windt, C. W., Vergeldt, F. J., De Jager, P. A., and As Henk, V., 2006, "MRI of Long-Distance Water Transport: A Comparison of the Phloem and Xylem Flow Characteristics and Dynamics in Poplar, Castor Bean, Tomato and Tobacco," Plant Cell Environ., **29**(9), pp. 1715–1729.

[21] Sprague, I. B., Byun, D., and Dutta, P., 2010, "Effects of Reactant Crossover and Electrode Dimensions on the Performance of a Microfluidic Based Laminar Flow Fuel Cell," Electrochim. Acta, **55**(28), pp. 8579–8589.

[22] Sprague, I. B., and Dutta, P., 2011, "Modeling of Diffuse Charge Effects in a Microfluidic Based Laminar Flow Fuel Cell," Numer. Heat Transfer Part A, **59**(1), pp. 1–27.

[23] Sprague, I., and Dutta, P., 2011, "Role of the Diffuse Layer in Acidic and Alkaline Fuel Cells," Electrochim. Acta, **56**(12), pp. 4518–4525.

[24] Thompson, M. V., and Holbrook, N. M., 2003, "Application of a Single-Solute Non-Steady-State Phloem Model to the Study of Long-Distance Assimilate Transport," J. Theor. Biol., **220**(4), pp. 419–455.

[25] Aharoni, N., and Lieberman, M., 1979, "Patterns of Ethylene Production in Senescing Leaves," Plant Physiol., **64**(5), pp. 796–800.

[26] Begg, J. E., and Turner, N. C., 1970, "Water Potential Gradients in Field Tobacco," Plant Physiol., **46**(2), pp. 343–346.

[27] Mullendore, D. L., Windt, C. W., Van As, H., and Knoblauch, M., 2010, "Sieve Tube Geometry in Relation to Phloem Flow," Plant Cell, **22**(3), pp. 579–593.

[28] Martre, P., Morillon, R., Barrieu, F., North, G. B., Nobel, P. S., and Chrispeels, M. J., 2002, "Plasma Membrane Aquaporins Play a Significant Role During Recovery From Water Deficit," Plant Physiol., **130**(4), pp. 2101–2110.

Downloaded From: http://nanoengineeringmedical.asmedigitalcollection.asme.org/ on 04/22/2014 Terms of Use: http://asme.org/terms